In situ DC electrical resistivity mapping performed in a reinforced concrete wharf using embedded sensors

Johann Priou, Yann Lecieux, Mathilde Chevreuil, Virginie Gaillard, Cyril Lupi, Dominique Leduc, Emmanuel Rozière, Romain Guyard, Franck Schoefs

In situ DC electrical resistivity mapping performed in a reinforced concrete wharf using embedded sensors.

Johann Priou[a] and Yann Lecieux[a*] and Mathilde Chevreuil[a] and Virginie Gaillard[b] and Cyril Lupi[a] and Dominique Leduc[a] and Emmanuel Rozière[c] and Romain Guyard [a] and Franck Schoefs[a]

[a]Laboratoire GeM (UMR 6183), Université de Nantes, CNRS, Centrale Nantes, 2, rue de la Houssinière, 44322 Nantes Cedex 3, France
[b] Laboratoire GeM (UMR 6183), ICAM, Département Génie Electrique, 35 Avenue du champ de Manœuvres, 44470 Carquefou, France
[c] Laboratoire GeM (UMR 6183), Centrale Nantes, CNRS, Université de Nantes, 1 Rue de la Noë, 44321 Nantes Cedex 3, France*

Abstract

Installation, calibration protocol and data analysis of multi-electrode sensors embedded in concrete are proposed in this study. Measurements of resistivity are performed in a port wharf and analyzed in parallel with measurements of humidity, temperature, and evolution of the mechanical strength of concrete. The correlation between the evolution of the compressive strength and the resistivity, allows to validate the measurement protocol proposed. To visualize the distribution of resistivities in the studied volume, pseudo-sections of apparent resistivity were displayed. A methodology to plot and use them as an indicator of corrosion adapted to civil engineering structures is proposed.

Keywords: Electrical DC resistivity, SHM, Embedded sensors, Coastal structures, Concrete

1. Introduction

The electrical resistivity quantifies the ability of a material to oppose the flow of electric current. This physical characteristic is related to the nature of the medium, its porosity and its electrolyte content. Direct Current (DC) electrical resistivity measurements have thus naturally been used for many years in geophysics to obtain subsoil images by tomography [1, 2] and estimate its constitution (type of rock, presence of water, trace of pollutant, etc.). In rocks the electric

*Corresponding author. Email: yann.lecieux@univ-nantes.fr

current propagates essentially through the open porosity by the intermediate of the interstitial fluids, generally water [3]. The electrolytic resistivity of rock is given by Archie's empirical law [4, 5]. The conduction via the pore solution of concrete can also be described by the Archie's law [6, 7]. Resistivity measurements are therefore also used in civil engineering for various applications. These include crack detection [8], porosity or mechanical strength monitoring [9], and concrete moisture content assessment [10, 11, 12]. Corrosion monitoring, the issue of interest in this study, is also an important field of application for resistivity measurement [13, 14, 15, 16]. The resistivity value is used as an indicator of the probability of corrosion. In the case of pitting corrosion induced by chlorides, it is possible, by calibrating the resistivity measurement, to assess the level of free chloride in a given concrete [10, 17, 18, 19, 20].

One hundred works and applications covering the field of resistivity measurement in concrete were identified in the reviews [21, 22]. Most of the experiments listed in [21] were carried out in the laboratory on test specimens without reinforcement bars.

Many measurement devices exist such as: discs, devices with 4 electrodes arranged in squares or aligned and most often interrogated with a Wenner protocol. There are also multi-electrode devices that allow, as in Geophysics, to display a resistivity section of the medium [23, 18, 24]. For on-site applications the most commonly used devices are portable Wenner probes for punctual measurement. Although simple to use and relatively inexpensive, they have two significant drawbacks. On the one hand, this system is suitable for punctual measurements as part of inspection campaigns. It is not designed to be integrated into a SHM (Structural Health Monitoring) measurement chain. On the other hand, the repeatability and reproducibility performances of these probes are lower than those observed with embedded devices. Coefficients of variations between 10% and 25% have been reported for variability measurements performed in specimens of the same batches and exposed identically [13, 25, 26, 18]. This dispersion has several origins, including the variability of the material and the variability of the contact resistance between the concrete surface and the measuring electrodes [27]. This observation shows the importance of the quality to bring to the electrical contact to ensure the reproducibility of the measurement. For this purpose it is more interesting to opt for an embedded sensor in order to improve the performances of the measuring system. It also offer the possibility to perform several measurements in the same location to avoid any bias due to material spatial variability of physical properties of concrete. This local variability is shown to have significant influence on resistivity measurement

due to the change of the path of current lines [27]. Spatial variability of chloride content [28] is also an issue.

To take full advantage of all the possibilities offered by electrical DC resistivity measurement [21, 22], current works must now focus on *in situ* installation of devices integrated into SHM measurement chain. These sensors should have the following characteristics:

- be embedded in concrete during the construction of the structure, to improve the repeatability of measurements, to get data in areas that are difficult to access and to follow the evolution from concreting to operation time;
- take into account the presence of reinforcement bars, either through a correction of the measurement [13, 29], or through a specific installation protocol [30];
- take temperature variations into account [31, 32, 24];
- give a large number of measurement points to decrease the amount of false alarm or bad detections [24, 33, 23, 18];
- obtain a mapping of resistivity in the concrete cover area [33, 23, 18] and better asses spatial variability.

The objective of this study is to propose a complete methodology for the installation and use of an on-site resistivity measurement device for the continuous monitoring of a reinforced concrete structure located in the splash zone of a marine environment, from its construction to its dismantling. The methodology addresses the following points:

- the *in situ* installation;
- the calibration protocol;
- the data analysis.

The section 2 is dedicated to the presentation of the sensors and their installation in a port wharf located at the mouth of the Loire river (on the west coast of France). Resistivity sensors (based on the technology used in the study [18]) were installed on two beams during the construction of the wharf together with temperature and humidity sensors. The sensors were installed within the framework of the project iMARECO2 (french acronym for Monitoring for

Maintenance, Reassessment and Optimal Design) managed by Keops Automation, with partners Université de Nantes, Nantes – Saint Nazaire Port and Bouygues Construction. It relies on the monitoring of a wharf during its construction, commissioned by Nantes – Saint Nazaire Port (Nantes – Saint Nazaire harbor, France). This section also describes concrete characterizations performed in laboratory. The principle of resistivity measurements with our sensors and their experimental validation are presented in section 3. The section 4 is the core of the analysis. It presents original developments on the adaptation of conventional methods used on geophysics to civil engineering structures, which allow the display and exploitation of apparent resistivity measurements. The last section, "results and discussion", is dedicated to the presentation of all the measurements (resistivity, humidity, temperature, compressive strength) and the correlations between the different measurements. The evolution of concrete at early age and then during the first year of the structure is monitored. The observation of phenomena related to concrete setting made it possible to validate measurement protocols and analysis methods, as well as to assess the *in situ* performances of the resistivity sensor and the measurement method proposed.

2. Material and Methods

2.1. Studied structure and measurement system

2.1.1. The wharf

The instrumented structure is a 350 meter long, 50 meter wide on pile wharf with a platform (slab and beams) in concrete. The structure is made of partly precast reinforced concrete elements (see Figure 1a). Precast elements are supported by 579 steel piles distributed over 10 longitudinal rows and 56 transverse rows (see Figure 1b). The precast elements are first laid down on the heads of steel piles. The junctions between these elements are reinforced with steel bars and then filled with concrete for ensuring the embedded connection. The concrete elements act as formwork for the structural parts of the wharf called "beams". Two beams at the end of the wharf are equipped with sensors. They are marked in Figure 1b.

2.1.2. Structural Health Monitoring (SHM) system for resistivity measurement

The wharf has been equipped with a multi-sensor system for the monitoring of concrete ageing. The measurement chain is designed to detect the long term penetration of chloride ions before it reaches the reinforcement and pitting corrosion begins. We are therefore particularly interested in the monitoring of concrete cover (see Figure 2a). The studied concrete elements are

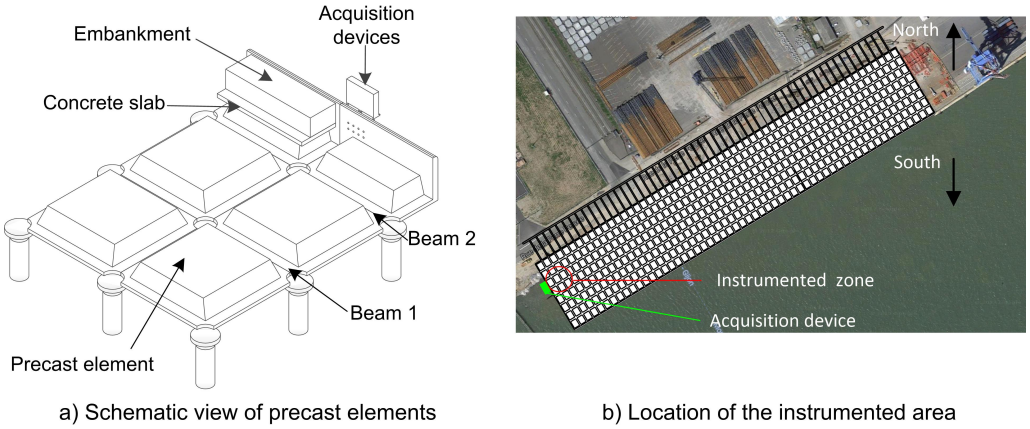

Figure 1: The wharf: building system and sensors location.

in the splash zone. Humidity, temperature and resistivity sensors were embedded in the concrete during the construction of the structure. They are located in each beams as shown in Figure 2.

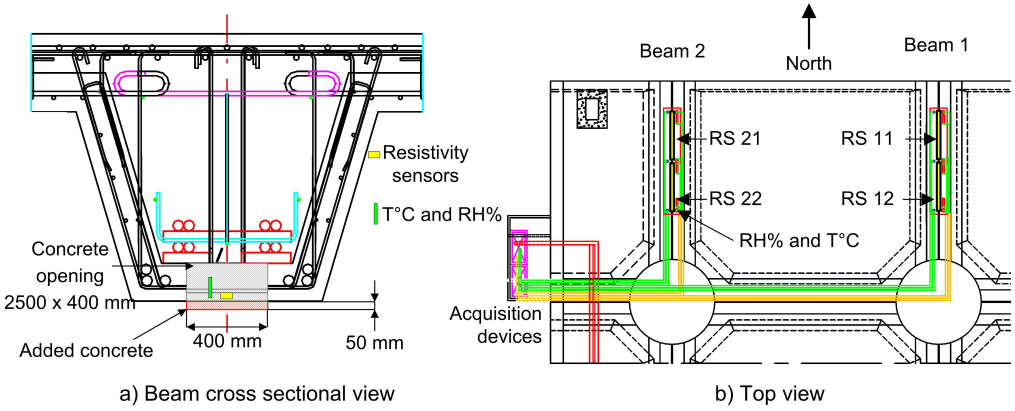

Figure 2: Location of resistivity sensors (referenced RS).

The lower part of each instrumented beam is equipped with:

- 2 resistivity sensors designed on the technology described in section 2.2;
- 3 combined humidity and temperature probes (ROTRONIC);
- 2 temperature probes Pt100.

Pt100 temperature sensors and humidity probes are positioned near resistivity sensors. Temperature sensors are used for the compensation of thermal effects on resistivity measurements.

They have also been used to determine the mechanical strength of *in situ* concrete using the maturity method. Position of these sensors are presented in Figure 3.

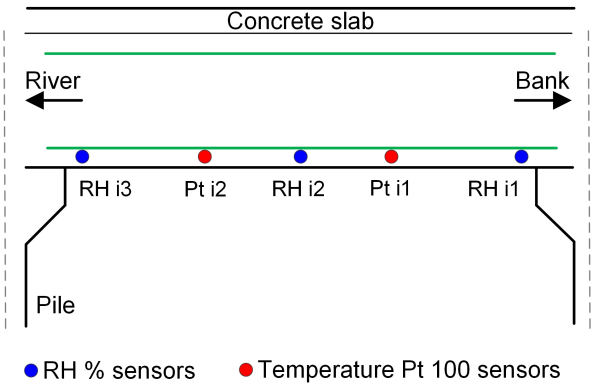

Figure 3: Schematic view of the longitudinal cross section of the beam: location of temperature and humidity sensors. The label $i = 1$ or 2 is the beam number.

Data acquisition for temperature and humidity sensors is carried out with a NI cDAQ-9133 acquisition unit. The whole installation (batteries, electronics, central unit, wires for resistivity measurement) allowing data acquisition has been integrated into waterproof boxes to protect it from external aggressions (wind, rain, tide, etc.). The boxes are positioned at the downstream end of the platform as shown in Figure 1.

2.2. The resistivity sensor and its acquisition device

The sensor embedded in the concrete structure consists of 32 electrodes in stainless steel spaced of $a = 35$ mm screwed into a 1.135 m long PVC bar. The exact dimensions of the sensors are visible in the Figure 4.

The resistivity measurements are performed punctually with a resistivimeter ABEM terrameter LS used by geophysicists which can also be used for civil engineering applications [18, 23]. The device injects current and measures potential differences on a line containing 4 to 32 electrodes in a user-defined sequence. Parameters such as the intensity of the current injected and the injection time are adjustable. The optimization of these parameters has been the subject of preliminary studies [18].

2.3. Proposed in situ installation of the resistivity sensor

The sensor installation has to meet the following operational constraints:

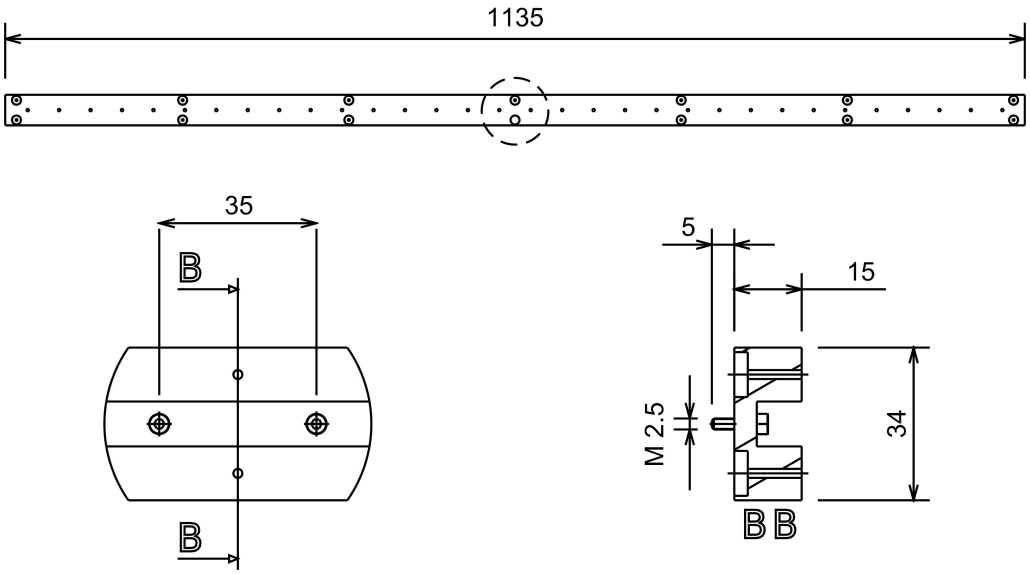

Figure 4: Sketch of the 32 electrode sensor. Dimensions are given in millimeters.

- First, the sensors must be placed in the center of the beams. This location required an opening on two prefabricated elements positioned side by side (see Figure 5a and 5b). The state of the structure before installation of the sensors is thus described in these figures 5a and 5b. The opening must then be filled with concrete poured into a formwork added to the structure after installation of the sensors (area drawn in red in Figure 5c);

- No electrical wires should run from the concrete bottom surface to the reinforcement to avoid creating a preferential path for seawater;

- The installation must be fast so as not to slow down the construction process;

- The sensor must probe the most relevant area. The concentration of chlorides is the highest in the zone located between 0 and 5 centimeters under the external concrete surface [10]. Cover concrete is then the zone where monitoring is the most interesting for early detection of chloride ion penetration in concrete and therefore detection of corrosion risk;

- The sensor must be insensitive to reinforcement bars. Indeed, the data analysis is based on a finite element (FE) simulation. If the sensor were sensitive to reinforcement bars, it would be necessary to accurately modelized these bars in order to take into account their

158 influences on the resistivity measurement. However, on site, the actual positioning of the
159 reinforcement bars is never exactly the same as planed. It would therefore be necessary
160 to perform an accurate position report of the actual reinforcement bars. Moreover, as the
161 reinforcement bars used are different according to the location within the beam, it would
162 be necessary to carry out a different FE model of the volume studied for each sensor.
163 Last, FE models representing reinforcements are complex and cannot be simplified. The
164 simulations would therefore be expensive in terms of calculation time.

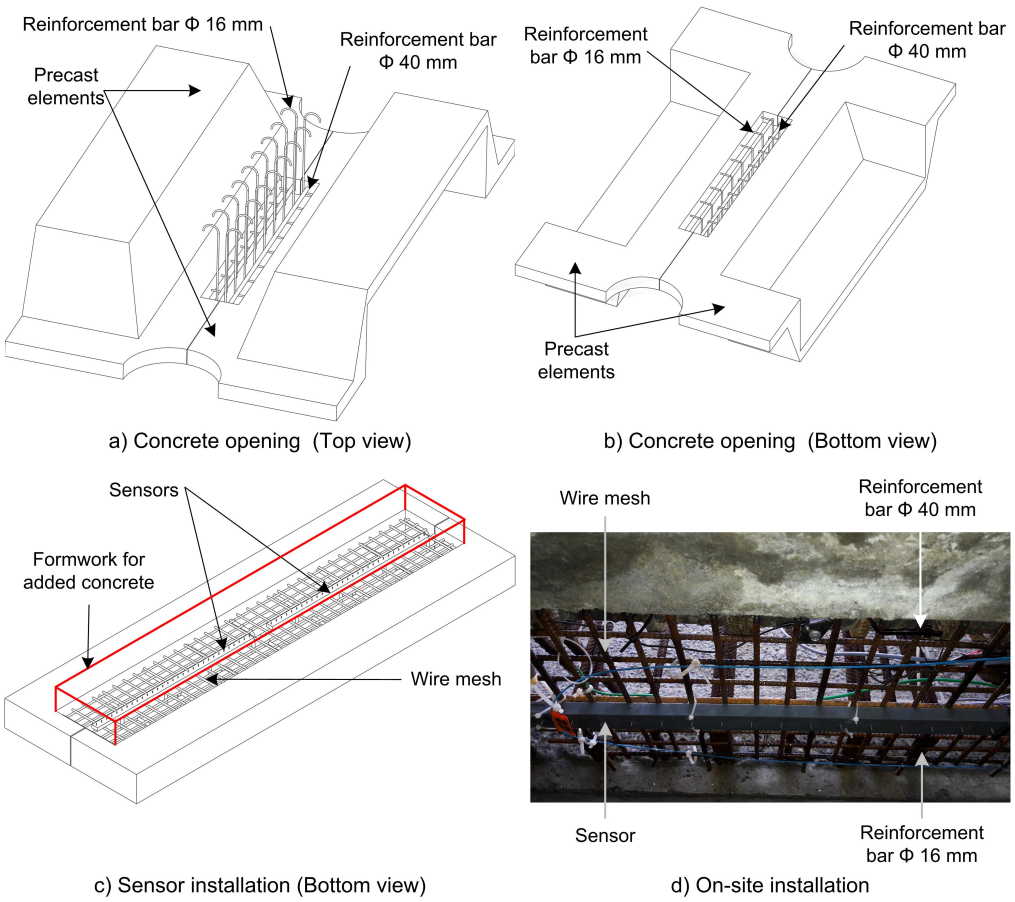

Figure 5: View of precasted concrete elements before (a and b) and after (c and d) the sensors are installed.

165 The technical solution chosen for the installation of the sensors, in agreement with all the
166 criteria listed above, consists in installing the two sensors on a welded wire mesh of the size of
167 the opening in the concrete (see Figure 5c). It was fixed on the 16 mm diameter reinforcements

168 visible on Figure 5d. The wire mesh is connected to the ground of the measuring instrument via
169 an electrical wire.

170 A welded wire mesh with a sufficiently fine mesh can be considered as a conductive plate.
171 Adding a conductive element between the reinforcement and the sensors confines the electrical
172 currents within the volume delimited by the concrete surface on the bottom side and the welded
173 mesh on the top side. The interest of the system is twofold. First, the resistivity measurement is
174 thus rendered insensitive to the presence of conductive elements (the reinforcement) located on
175 the other side of the conductive plate. Secondly, the volume surveyed using resistivy measure-
176 ments is simple to modelize, since it is a rectangular volume without reinforcements except the
177 welded mesh (see volume in red in Figure 5c).

178 On site, however, it is not possible to install a metal plate or very dense mesh. The meshes
179 must be wide enough to allow the aggregates and the needle to vibrate the concrete to pass
180 through. A 35 mm mesh could be installed on site. A numerical sensitivity analysis performed
181 with a model of the welded mesh and presented in the section 4 demonstrates that the mesh
182 size used here is acceptable to avoid that the reinforcement bars influence the measurements of
183 resistivity in cover concrete.

184 *2.4. Materials and mixture used on-site*

185 The composition of cast-in-place concrete is given in Table 1. The strength class was C40/50
186 and the mixture complied with the requirements of French Standard NF EN 206-1 for XA2
187 exposure class; i.e. minimum binder content of 350 kg/m^3 and maximum Effective water to
188 Binder (Weff/Beq) ratio of 0.50. Portland cement CEM I 52.5 N SR3 was used to provide sulfate
resistance. The actual Weff/Beq ratio was 0.45.

	Content (kg/m^3)
Gravel 11/22	740
Gravel 2/10	300
Sand 0/4	810
Cement CEM I 52.5 N SR3 (C)	360
Plasticizer	3.8
Water effective	161

Table 1: Composition of concrete mix

189

2.5. Characterization of concrete performed in laboratory environment

In addition to the measurements carried out on site, laboratory tests were performed in order to get key properties of the concrete. The day when the beams were casted, 40 cylindrical samples of 110 mm diameter and 220 mm height were made with the same concrete and at the same time. After one day, they were stored in water at 3 different temperatures, 10 °C, 20 °C and 40 °C. The aim of the characterization tests was to obtain:

- the porosity accessible to water;
- the compressive strength;
- the equivalent age.

Permeability is an indicator of concrete durability since it controls the rate at which aggressive agents such as ions in sea water can penetrate into concrete. Number of scientific studies underline the strong correlation between the porosity of a concrete and its permeability [34, 35]. When porosity is reduced, permeability also decreases. Porosity is thus an essential characteristic of reinforced concrete [36]. In this study, water porosity was assessed after 90-day wet curing on three concrete discs by the vacuum water saturation method, according to French standard NF P18-459. An interesting feature of the resistivity comes from its link to porosity since porosity evolves with hydration [37]. Porosity decreases during the first 90 days leading to an increase in resistivity. At the same time, the mechanical strength of concrete is influenced by porosity. Resistivity measurement can thus be considered as an interesting indicator of durability [38] and material hardening. Thus, in section 5, resistivity measurements are compared with porosity measurements. Then, the evolution of the *in situ* mechanical strength is computed at an equivalent age.

Compressive strength characterization was also carried out in laboratory. The compressive strength was measured at 1, 2, 7 and 28 days on the specimens stored in water at 10°C, 20°C and 40 °C. 30 specimens were tested, i.e. 3 specimens on day 1 and 3 specimens for each temperature range on days 2, 7 and 28. The objective of these tests was to assess the compressive strength of the concrete of the *in situ* structure. For this purpose, the maturometry technique was used. It aims at the computation of the age of an on-site concrete equivalent to a concrete stored in the laboratory at a reference temperature $T_{\text{ref}} = 20$ °C. This calculation requires knowledge of the thermal history of the structure (measured with PT100 probes) [39, 40]. Maturometry is firstly

based on the fact that the compressive strength of concrete depends only on its temperature. For a constant temperature, the mechanical strength of concrete can be described by the following expression [41]:

$$f_c(\tau; T, T_{\text{ref}}) = f_{c28\text{d}}(T_{\text{ref}})\text{e}^{s(T_{\text{ref}})\left(1-\sqrt{\frac{28}{\tau(t;T,T_{\text{ref}})}}\right)} \tag{1}$$

where τ is the age of the concrete in days for the reference temperature T_{ref} or the equivalent age for a temperature $T \neq T_{\text{ref}}$, s the adjustable parameter and $f_{c28\text{d}}$ the compressive strength assessed at 28 days and at the reference temperature, here chosen $T_{\text{ref}} = 20$ °C.

Secondly, the sensitivity of concrete hardening to temperature is given by Arrhenius law, whose unique parameter E_a called apparent activation energy [J/mol] characterizes the curing of a concrete. The activation energy is related to the equivalent age of the concrete and its thermal history by the following relationship (2) [42]:

$$\tau(t; T, T_{\text{ref}}) = \int_0^t \text{e}^{-\frac{E_a}{R}\left[\frac{1}{T(\theta)}-\frac{1}{T_{\text{ref}}}\right]}\text{d}\theta \tag{2}$$

where t is the considered time period (days), R is the gas constant 8.314 J/mol.K and T (K) is the average absolute temperature of concrete.

It is thus possible to calculate the apparent activation energy of a concrete from the mechanical strength of the material stored at different temperatures following these steps:

- First, parameter s in equation (1) is determined from the mechanical strength curve of the samples stored at $T_{\text{ref}} = 20$ °C;
- In a second step, the parameter E_a is calculated in such a way as to minimize the difference between the compressive strength measurement at 10 °C and 40 °C considering equivalent age computed with equation (2) and the model of the equation (1);
- Once E_a has been determined, the equivalent age of the actual structure can be determined at any point on the structure equipped with a temperature probe;
- Then, it is possible to calculate the mechanical strength of the real concrete at a given time with equation (2) using experimental data collected in laboratory and on-site temperature measurement.

3. Resistivity measurement: protocol and performance assessment within the framework of the *in situ* installation

3.1. Principle and protocol

The resistivity measurement technique used in this study is the direct current electrical tomography method. It is commonly used in the field of geophysics [1]. This measurement technique consists in successively using several sets of four surface electrodes to obtain one resistivity measurement. Two electrodes are used to inject an electric current into the studied volume. These two electrodes are respectively labelled A (injected current I) and B (injected current -I) (see Figure 6). The other two electrodes labelled M and N are used to measure a potential difference ΔV.

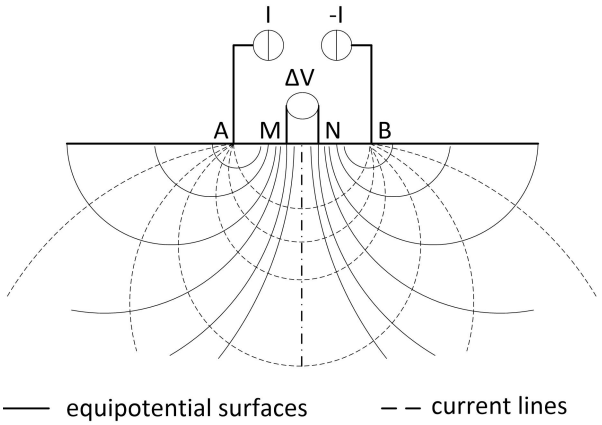

Figure 6: Principle of the resistivity measurement with a four electrode device. The equipotential surfaces drawn on the Figure correspond to a semi-infinite homogeneous medium.

For a homogeneous medium of resistivity ρ (Ωm), the relationship between the imposed current I, the potential difference ΔV and the resistivity is given by equation (3):

$$\rho_{app} = G\frac{\Delta V}{I} \tag{3}$$

where G (1/m) is the geometric factor. This geometric factor is only function of the interrogation protocol (Wenner alpha, beta, gamma, Schlumberger, Dipole-Dipole) and of the geometry of the studied volume. In geophysics, the medium is assumed to be semi infinite. In this case, G depends only on the distance between the electrodes of the considered quadripole. For a Wenner alpha protocol, AM = MN = NB = a, thus $G = 2\pi a$. The factor $2\pi a$ is also the one used for the analysis of potential measurement performed with a portable resistivity probe. However, if the

medium is not semi-infinite, (for instance in in civil engineering in beams or slabs), G depends also on the specimen geometry. In such a case, the G factor has to be evaluated numerically or experimentally.

Finally, when the medium is not homogeneous, the resistivity, calculated from equation (3) is called apparent resistivity. The 32 electrodes of the sensor allow $m = 129$ measurements with the Wenner alpha protocol. The corresponding sequence is given on Figure 7.

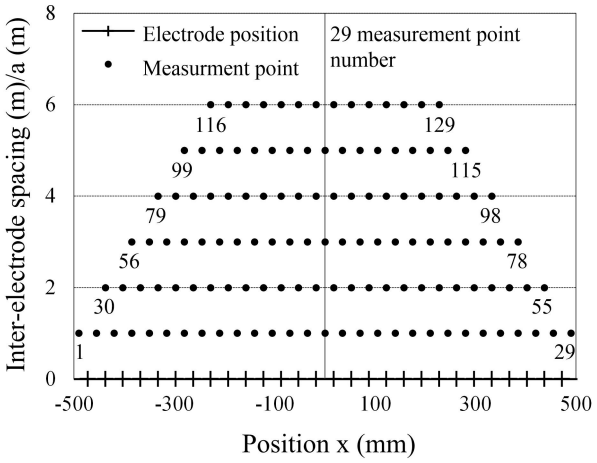

Figure 7: Graphical representation of the Wenner alpha protocol measurement points with respect to the positions of the 32 electrodes.

From the m experimental or numerical measurements we deduce the geometric factors $G^j = \rho \frac{I}{\Delta V^j}$, for $j = 1, \ldots, m$. These are used to define the measured apparent resistivities $\rho^j_{app} = G^j \frac{\Delta V^j}{I}$ linked to the j^{th} measurement.

Resistivity measurements were performed during 18 months, several times a week during the first weeks in order to observe the evolution of concrete at early age. Further measurements are planned during next years but on a half-yearly basis. From all these measurements a resistivity mapping is obtained. It represents the apparent resistivity of the volume located under the measuring electrodes and it is called pseudo-section of apparent resistivity.

3.2. Assesment of measurement repeatability and trueness in laboratory and in situ

The quantification of measurement uncertainties is necessary, especially in civil engineering since concrete is a heterogeneous medium. Thus, the repeatability of the resistivity measurements was evaluated on site within concrete and in a homogeneous environment of constant

resistivity but including the same welded mesh as for the on-site installation. A model of the volume of concrete studied on site was reproduced for laboratory tests (volume in red in Figure 5c). A wooden mould was equipped with a welded mesh and a resistivity sensor identical to those embedded on site in the concrete beams. The volume was filled with water maintained at a constant temperature of 20° C. The resistivity of water was obtained using a conductivity probe considered as the reference. Five repeatability tests have been performed for each of the m =129 measurement points $\{M^j\}_{j=1}^{m}$ (Figure 7). The repeatability error is computed as the coefficient of variation of the sample $\widetilde{\rho}^j = \{\rho_{app,k}(M^j)\}_{k=1}^{5}$ containing the 5 values of the repeatability test:

$$\mathrm{CoV}(\widetilde{\rho}^j) = \frac{\sqrt{\mathrm{Var}(\widetilde{\rho}^j)}}{\bar{\rho}^j}, \; j \in \{1, \ldots, m\} \tag{4}$$

where $\bar{\rho}^j$ and $\mathrm{Var}(\widetilde{\rho}^j)$ are the mean value and the variance of the sample $\widetilde{\rho}^j$. Repeatability tests were performed in water of variable resistivity. The resistivity values [23, 92 Ωm] are chosen to match with the values expected to be measured on site. The value of about 20 Ωm is expected for a concrete at early age while 100 Ωm could be the resistivity value of a concrete with a high water saturation after few weeks. The results are plotted on Figure 8 with respect to the sequence of measurement points presented in Figure 7.

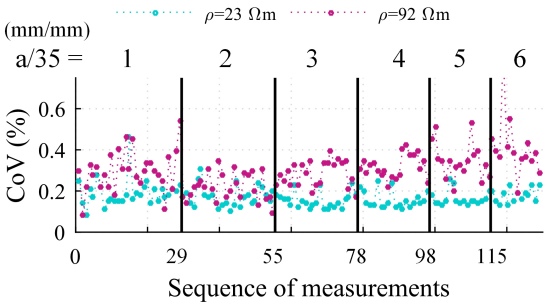

Figure 8: Coefficients of variation $\mathrm{CoV}(\widetilde{\rho}^j)$ of the m = 129 measurements for tests performed in water using 10 mA current injection.

The coefficients of variation are very low in both cases since they are less than 0.55 % (except the value of 0.87 for one measurement) and close to those found in [25]. It should be noted that after one year, the average value of the resistivity measured on site was less than 100 Ωm and consequently, the input parameters of the device (injected current, time of injection, protocol,etc.) are adapted. Similarly, repeatability tests conducted on the wharf made it possible to evaluate the performance of the *in situ* device as shown in Figure 9.

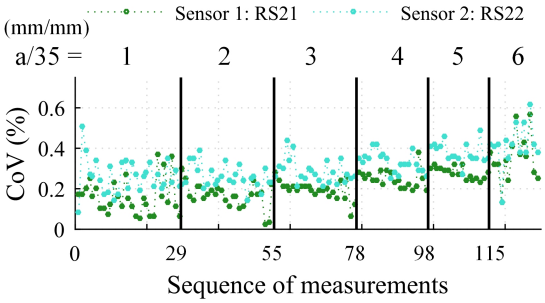

Figure 9: Coefficient of variation $\mathrm{CoV}(\widetilde{\rho}^j)$ of the $m = 129$ measurements for tests performed *in situ* using 10 mA current injection.

The value of the coefficient of variation recorded on site is slightly higher than that observed in the laboratory, but remains very low (less than 0.6 %). The difference is explained by the presence of more sources of uncertainties *in situ*, including variations in contact resistance or poor compensation for thermal effects. It is also possible to assess the accuracy error but only for measurement performed in water and using the geometric factor computed numerically. For a set of 5 repeatability tests, a reference value is given by the conductivity probe $\hat{\rho}$. The bias is computed using the equation (5):

$$b^j = |\hat{\rho} - \bar{\rho}^j|. \tag{5}$$

The bias also represents the trueness error in this case. It represents in particular the error on the modelling performed using the direct finite element model since the bias is related to an approximate numerical evaluation of the geometric coefficient G. The results obtained confirm the global relevance of our finite element model (see section 4) since the relative bias is low (in average 0.7 Ωm for the medium of 23 Ωm and 2.4 Ωm for the medium of 92 Ωm) except for 12 measurement points (see Figure 10). The latter are those made with the electrodes at the ends of the sensor. This means that FE modelling does not correctly predict the propagation of current near the lateral edges of the sensor with this geometric configuration. Consequently, in the rest of the study, in order to avoid misinterpretations this measures were removed from the database. Finally 117 measurement will be kept (129 minus 12 measurements, *i.e.* two measurements at each end of the sensor for a given spacing, considering 6 different spacings).

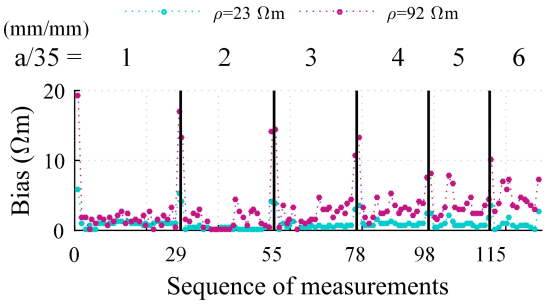

Figure 10: Relative biais b^j of the $m = 129$ measured apparent resistivities for tests performed in water using 10 mA current injection.

4. Mapping of resistivity measurements

The set of m=117 resistivity measurements obtained for a given time period allow three levels of analysis to be performed:

- The average apparent resistivity representative of the material is estimated from a large number of measurements performed in a small volume. The dispersion of the measurements reflects the heterogeneity of the concrete. The average value is useful information for the monitoring of hardening concrete (see section 5). By testing a material containing a given chloride content [20, 18] it is also possible to estimate a probability of detection of an average free chloride content in the survey area by knowing both average apparent resistivity value and dispersion of the measurements;

- The measurements can be displayed directly through a pseudo section of apparent resistivity. It does not require numerical inversion and thus allows an instant display of the measurement results. It is then possible to visualize areas for which the resistivity varies between two measurement campaigns as well as gradient effects due to chloride and humidity. Apparent resistivity is also useful for calculating the true resistivity obtained by reverse analysis. Indeed, in all algorithms currently in use, the initial value of true resistivity is the apparent resistivity.

- The true resistivity obtained by inversion allows the exact location of areas of variable resistivity. However, there is currently no algorithm available to quickly and reliably reverse apparent resistivity measurements for *in situ* use applied to civil engineering structures [43]. This point has not been addressed in the context of this paper, whose subject is

the development of tools usable *in situ* or in a supervision program (i.e. without reverse analysis).

The objective of this section is to propose a method for obtaining pseudo-sections of apparent resistivity in the context of a measurement carried out on a reinforced concrete structure. The methodology used is strongly inspired by the techniques used in the field of geophysics. The methods applied in this context are briefly described and the necessary adaptations to the field of civil engineering highlighted.

4.1. Apparent resistivity in geophysics: practice and limits

In geophysics, the measurements of the electric potential differences are displayed through the apparent resistivity defined with equation (3) where the geometric factor G is determined so that the apparent resistivity is equal to the true resistivity when the medium is homogeneous. In the case of the semi-infinite medium as it is encountered in geophysics, the geometric factor can be defined analytically (see section 3.1). When the studied space is not homogeneous, the apparent resistivity gives only an approximate representation of the true resistivity [3, 2].

The apparent resistivity is displayed in the 2D space at data points with cartesian coordinates (x, z). The x-coordinate is obtained with the x positions of the electrodes, for instance for a Wenner device, x is the middle of the 4 electrodes. The z-coordinate is defined with a sensitivity analysis based on the Frechet derivatives. The sensitivity is studied as a function of the depth. By convention, the z-coordinate value corresponds to the depth (or distance to the sensor) where half of the Frechet derivative integral is obtained.

In the present study, the medium is not semi-infinite and consequently, first we have to assess the geometric factor, and second we cannot compute the Frechet derivatives. We thus propose to assess the geometric factor by considering the geometry of the monitored domain and the presence of the wire mesh and the sensor (see section 4.3.1) and we propose an approach, that mimics the analytical approach where the apparent resistivity coefficients result from a sensitivity analysis using an approximation of the solution of the resistivity problem (section 4.2).

4.2. Proposed methodology for displaying the apparent resistivity for any geometry

4.2.1. Parametrization

In this section, we propose a methodology to display the apparent resistivity for any electrostatic problem. It is based on a sensitivity analysis of the electric potential differences with

respect to the resistivity where the resistivity is simply modeled with constant coefficients by blocks. Let ρ_i with $i \in I = (1, \cdots, d)$ be the resistivity coefficients allocated to the d disjointed blocks of the medium and let ΔV^j, $j = 1, \cdots, m$, the electric potential differences that solve the electrostatic problem using this parametrization. By considering a finite range of possible values for each resistivity coefficient, we introduce sensitivity indices that quantify the part of the variance of ΔV^j due to the variability of ρ_i and that are derived from the Sobol indices $\frac{\mathrm{Var}(\mathbb{E}(\Delta V^j|\rho_i))}{\mathrm{Var}(\Delta V^j)}$. In this expression, the conditional expectation $\mathbb{E}(\Delta V^j|\rho_i)$ represents the function of ρ_i only which best approximates ΔV^j, its variance $\mathrm{Var}(\mathbb{E}(\Delta V^j|\rho_i))$ thus measures the fluctuation of ΔV^j as if it were a function of ρ_i only, and it is normalized by the total fluctuation of ΔV [44]. Here we rather use indices normalized with the maximal variance of the potential differences to better consider the most influenced measures:

$$S_i^j = \frac{\mathrm{Var}(\mathbb{E}(\Delta V^j|\rho_i))}{\max_{l=1,\ldots,m}(\mathrm{Var}(\Delta V^l))}. \tag{6}$$

The sensitivity indices can be computed using Monte Carlo simulation methods [45] or using approximations of ΔV^j on functional bases [46].

The blocks are sized so to have an equivalent influence over the measurements, *i.e.* such that $S_i = \sum_{j=1}^m S_i^j$ are of the same order for all of the blocks $i \in I$.

4.2.2. Calculation and display of the resistivity

We finally define the apparent resistivity $\rho_{app,i}$ displayed in block i as a weighted sum of the measured apparent resistivities with respect to the sensitivity indices:

$$\rho_{app,i} = \frac{\sum_{j=1}^m \mathrm{S}_i^j \rho_{app}^j}{\sum_{j=1}^m \mathrm{S}_i^j} \tag{7}$$

with ρ_{app}^j the measured apparent resistivity related to the measured electricity potentials ΔV^j with the relation (3) in which the geometric factor G is determined *a priori* for the studied case.

4.3. Towards the application on the concrete structure: preprocessed parameters for the display of the apparent resistivity

4.3.1. Determination of the geometric factor

As mentioned above, the geometric factor G first needs to be determined acoording to equation (3). For the case of the concrete structure studied in the present paper, the geometric factor has been estimated using the geometry and boundary conditions of the surveyed part of the concrete structure, that includes the added concrete marked out in red on Figures 2 and 5 and the

layer of concrete containing the wire mesh and the sensor. A finite element model reproducing these conditions was used to assess the geometric factor.

Let denote Ω the domain occupied by the medium. Its boundary is composed of the outer boundary of the parallelepipedic domain and of the boundaries in contact with the wire mesh and the sensor the geometries of which are modeled faithfully. The electric potential is the solution of problem (8):

$$\begin{aligned}
&\nabla.\left(-\frac{1}{\rho}\overrightarrow{\nabla}V\right) + \delta_A I - \delta_B I = 0 \quad \text{in the medium,}\\
&-\frac{1}{\rho}\overrightarrow{\nabla}V.\vec{n} = 0 \quad \text{on the outer boundary of the domain,}\\
&-\frac{1}{\rho}\overrightarrow{\nabla}V.\vec{n} = 0 \quad \text{on the boundary of the sensor,}\\
&V = 0 \qquad\qquad \text{on the boundary of the wire mesh,}
\end{aligned} \tag{8}$$

where ρ is the resistivity and $\delta_A I$ and $\delta_B I$ are punctual sources of electric current I and $-I$ imposed by the electrodes at points A and B.

For the determination of the geometric factors, we consider a homogeneous medium of known resistivity ρ and impose a current intensity $I = 1$ A. We then compute the electric potential differences $\{\Delta V^j\}_{j=1}^m$ for the $m = 117$ positions of the electrodes with the Wenner device from which we deduce the geometric factors $\{G^j\}_{j=1}^m$.

4.3.2. Parametrization of the numerical model

We consider the *in situ* concrete structure. Problem (8) is solved using the finite element method. The resistivity is now considered non homogeneous and modeled with a piecewise constant resistivity as presented in section 4.2.1 where the blocks are chosen so that the measurements are equally sensitive to each block. Figure 11 shows an example of the distribution of the blocks for modeling the resistivity. The further the layers are from the sensor, the less influent they are on the potential differential and thus the larger are the blocks. For the purpose of the study which concerns the detection of a chloride front, we assume a uniform resistivity with respect to the y-axis. A single block along the y-axis to which we affect the resistivity identified underneath the sensor (the surveyed area) is sufficient to model the medium.

The parameters of the problem used in the following sections are the resistivities of the blocks.

To illustrate the importance of considering the true geometry for defining the z-coordinate to display the apparent resistivity, we compare the sensitivities of the electric potential differences

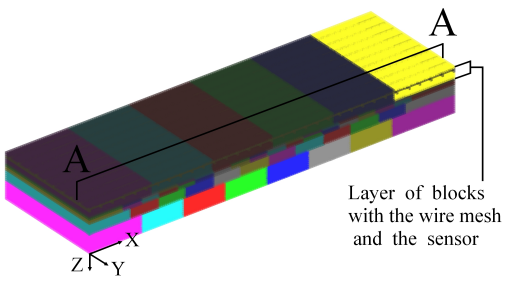

Figure 11: Model of the monitored concrete structure: example of distribution of the blocks for the modeling of the resistivity with equivalent influence on the measurements.

obtained in both cases: analytically with the Frechet derivatives on the semi-infinite medium and numerically on the more realistic geometry of the surveyed part of the concrete structure presented above. Figure 12 shows the sensitivities for three different distances of the electrodes: 35 mm (top Figure), 70 mm (middle Figure) and 105 mm (bottom Figure). The depth at which the apparent resistivity is displayed using the Frechet Derivatives Sensitivities (FDS) of the semi-infinite case, that is half of the integral of the sensitivity curve, is represented with a solid red line. The one obtained numerically by considering the more realistic geometry is represented with a dashed red line. For close distances of 35 mm both sensitivities are in good agreements whereas the electrodes are distant, the numerical sensitivity has a bimodal distribution contrary to the semi-infinite case. This shows that we do not probe the medium only far away from the sensor but also the medium close to the sensor. This is due to the actual conditions of the surveyed area especially that of the underside of the concrete.

Since the part of the structure containing the steel reinforcement above the wire mesh is not part of the structure we want to study, the numerical model is also used to make sure the sensor is not sensitive to that upper part (and so not sensitive to the steel reinforcement), or in other words to make sure that the 35 mm wire mesh is well designed to prevent current from flowing to the other side of the wire mesh. To that aim, we have considered an enlarged domain of concrete by adding a layer of concrete above the wire mesh in the numerical model and we have analyzed its effects on the electric potential differences. Figure 13 shows the modeling with the layer of concrete above the wire mesh. The electric potential differences is sensitive to the lower part of the domain with a sensitivity index $S_{lower} \approx 1$ and to the upper part of the domain with a sensitivity index $S_{upper} \approx 2.10^{-8}$ assessed numerically. The experimental setup thus fulfills the

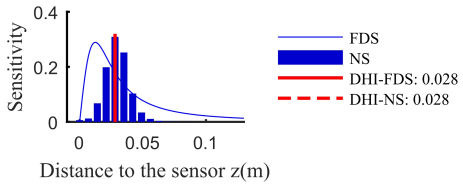

a) Sensitivity for a 35 mm distance between electrodes

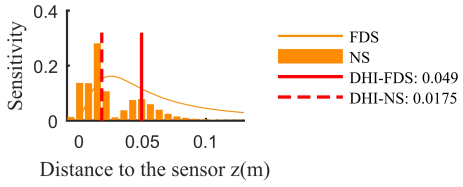

b) Sensitivity for a 70 mm distance between electrodes

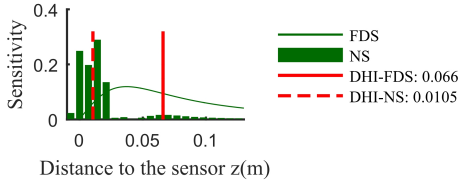

c) Sensitivity for a 108 mm distance between electrodes

Figure 12: Sensitivity of the measurement with respect to the depth obtained analytically on the semi-infinite medium (FDS: Frechet Derivatives Sensitivity) and numerically on the more realistic geometry (NS: Numerical sensitivity). The red lines locate the half of the integral of the sensitivity (DHI).

requirements.

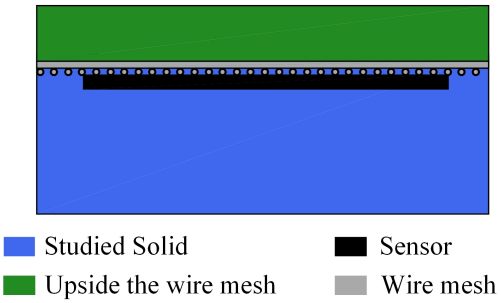

Figure 13: Section A-A of the model used to study the influence of the part above the wire mesh.

4.4. Validation of the method for displaying of the apparent resistivity

The method is validated on experimental and numerical cases for which the resistivity field is known *a priori*. The displayed apparent resistivity obtained with the proposed method is viewed to verify the similarity between the imposed and the displayed apparent resistivities first in a homogeneous medium and then in non homogeneous ones. In the following, the resistivity is displayed in the 2D section A-A drawn in Figure 11. The ordinate axis will correspond to the distance to the underside of the monitored concrete part and is equal to $h - z$, with z the distance to the sensor (as in section 4.1) and $h = 0.12$ m the distance of the sensor to the underside.

4.4.1. Tests on homogeneous medium

Let first consider the numerical model governed by equations (8) with constant resistivity $\rho = 80\,\Omega$m in the whole domain. The apparent resistivity coefficients $\rho_{app,i}$ (Figure 14b) obtained with equation (7) for 62 blocks and using the geometric factors assessed numerically is compared to the imposed homogeneous resistivity (Figure 14a). As expected, looking at the displayed apparent resistivity $\rho_{app,i}$ in the homogeneous case, the uniform resistivity is recovered to the machine precision.

On Figure 14a, the dashed line defines the domain, joined underneath the sensor, the resistivity of which is the most influent on the measurements of electrical potential differences. As the outer part is not influent on the measurements, it is removed from the plots in the following.

Same comparison is performed on two experimental cases with supposed homogeneous source water of resistivity 23 Ωm and mixture of source and distilled water of resistivity 92 Ωm. Figure 15 displays the apparent resistivities $\rho_{app,i}$ obtained with equation (7) for 46 blocks

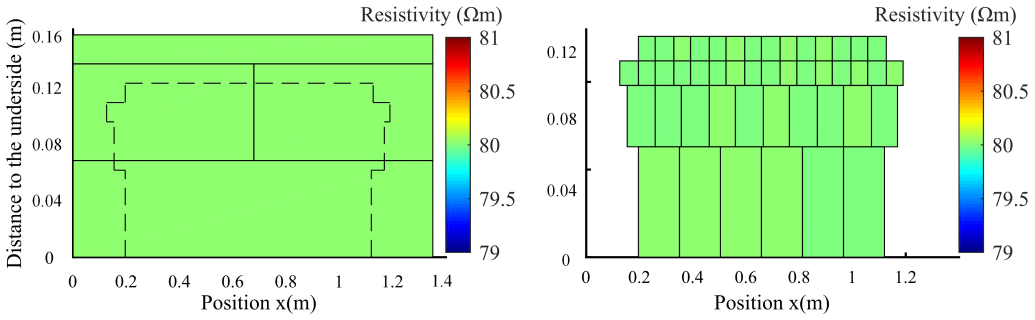

a) Imposed resistivity on the FE model

b) Corresponding map of apparent resistivity

Figure 14: (a) Original resistivity imposed on the finite element model. (b) Pseudo section of apparent resistivity display by the method.

in the influent domain. Figures 15a and b plot the results for the medium of resistivity 23 Ωm and 92 Ωm respectively. Again in both cases the apparent resistivity is similar to the homogeneous resistivity of the water.

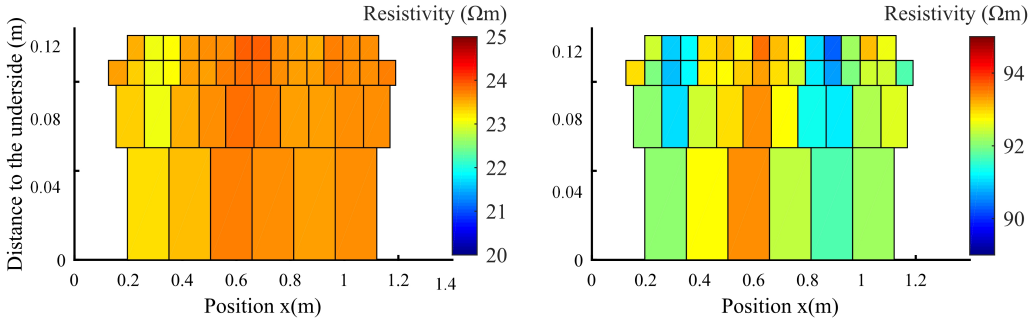

a) Apparent resistivity for a 23 Ωm water

b) Apparent resistivity for a 92 Ωm water

Figure 15: Pseudo section of resistivity for homogeneous mixtures of water. (a) source water with resistivity 23 Ωm and (b) mixture of source and distilled water with resistivity 92 Ωm.

4.4.2. Heterogeneous medium

Additional tests have been carried out on the numerical model with known imposed non homogeneous resistivity field. Figures 16 and 17 present results of the display method on two cases where the imposed resistivities have vertical and horizontal gradients respectively (left Figures). The corresponding displayed apparent resistivity $\rho_{app,i}$ (right Figures) for 46 blocks in the influential domain are plotted in the right Figures. Although the values of the original resistivities are not exactly recovered because of the heterogeneity of the resistivity field, the

display method is able to catch the trends of the original resistivity. The proposed display method is found efficient as these results are consistent with those obtained in geophysics in semi-infinite media and using Frechet Derivatives.

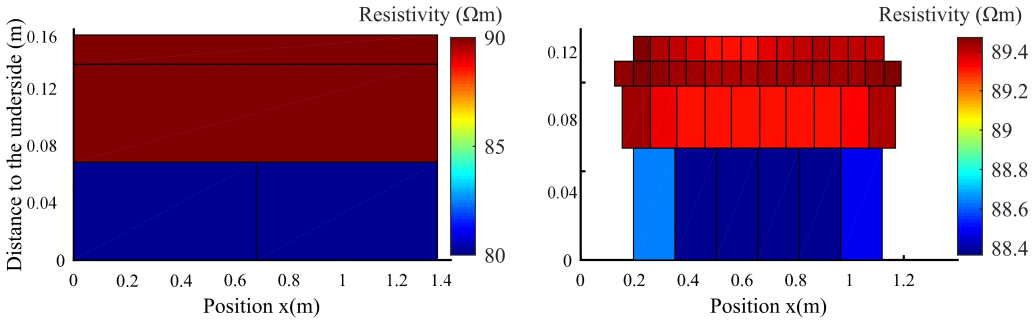

a) Imposed resistivity on the FE model

b) Corresponding map of apparent resistivity

Figure 16: Original resistivity with vertical gradient imposed on the finite element model (a) and corresponding map of apparent resistivity displayed by the proposed method (b).

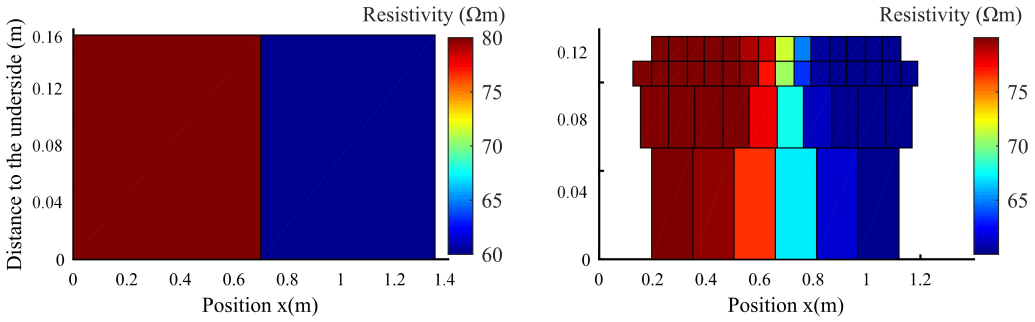

a) Imposed resistivity on the FE model

b) Corresponding map of apparent resistivity

Figure 17: Original resistivity with horizontal gradient imposed on the finite element model (a) and corresponding map of apparent resistivity displayed by the proposed method (b).

The mapping for displaying the apparent resistivity could also be adapted to other parametrization methods. For instance one can refine the block distribution of the apparent resistivity but the computation cost becomes quickly unaffordable when the number of parameters increases.

5. Results and discussion

5.1. In situ Monitoring of temperature and humidity

The on-site temperature measurement is a crucial data needed for the correction of the resistivity measurements [31, 32, 24] and an input for the maturity method. Figure 19 gives the

evolution of the temperature during the whole duration of the study. The measurements of the 3 sensors Pt11, Pt12 and Pt13 are very close showing a homogeneous distribution of the temperature along the beam. Daily variations (day-night cycles) and seasonal variations are visible respectively on Figures 18 and 19. On the same beam, the relative humidity measured in concrete in the lower zone is shown in Figure 18 and Figure 19.

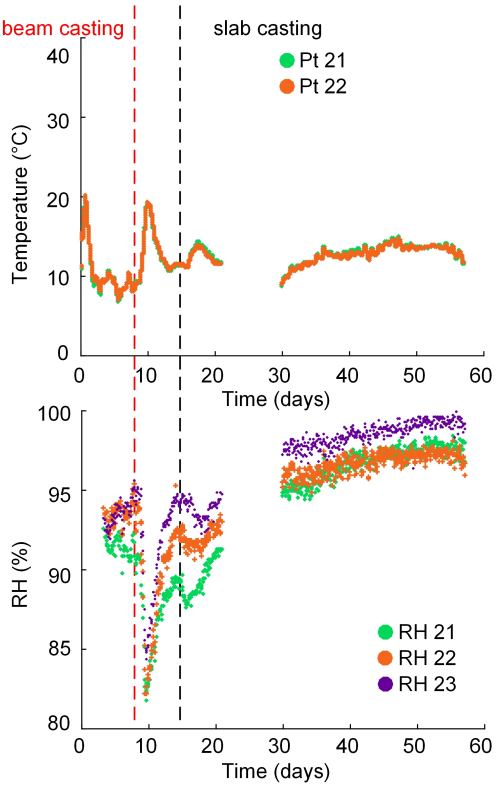

Figure 18: Monitoring of temperature and relative humidity (RH) in beam 2 with time (0 to 60 days).

The structure was cast in three steps. The part containing the sensors was filled on day 0 and a first temperature peak appears about 12 hours later (see Figure 18). The central part of the beam was cast 9 days later. This operation is visible in Figure 18 where a second temperature peak reaches 20°C. Finally, a few days later, the slab is cast, which has the effect of slightly modifying the temperature in the lower part of the beam.

Relative humidity records begin 48 hours after concrete casting in the lower part of the beam. The humidity probes are positioned in concrete openings recapped immediately after insertion

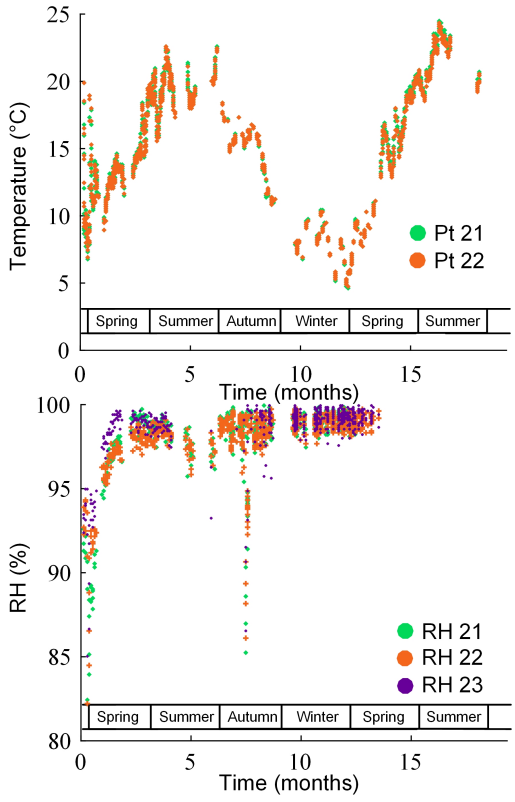

Figure 19: Monitoring of temperature and relative humidity (RH) within beam 2 with time (0 to 18 months).

of the sensors. It is therefore a measure of the relative humidity inside a cavity of a few cubic centimeters (about 10 cm^3) in the concrete, but not a direct measure of water content in the porosity. The main information is that despite of temporary decreases, linked to the occasional rise in temperature (during chemical reaction of the cement paste), the relative humidity increases in the cavity to stabilize around 98% on day 50 (see Figure 18) then remains between 95 and 100% (Figure 19). The water content of concrete is high as the underside elements of the structure are regularly submerged or splashed during tidal cycles. A decrease of this relative humidity to 95% occured during the first summer (see Figure 19). This is an important indication that should be taken into account when analyzing resistivity measurements. Indeed, a concrete with a high water content naturally has a low resistivity.

5.2. Material parameters

5.2.1. Porosity

The porosity of the concrete used *in situ* has been estimated at 12% accoording to the French standard NF P18-459 as mentionned in section 2.5. This porosity value is relatively low [36]. Porosity is one of main general durability indicators that can be used to estimate the durability of concrete strcutures exposed to chlorides. The determination of porosity is actually necessary to deduce the water saturation of concrete and its chloride content.

5.2.2. Compressive strength

To determine the activation energy, following equation (1), data are analyzed at the end of the first day, since during 24 hours all specimens have been stored at the same temperature. Figure 20 shows the influence of the curing temperature on the compressive strength and Figure 21 shows the time-temperature transformation based on the calculation of equivalent age. The bars on the graph represent the standard deviation of three experimental measurements.

The value of activation energy E_a deduced from the superposition method was 24.4 kJ/mol. This value was used to assess equivalent time $\tau(t; T, T_{ref})$ with $T_{ref} = 20$ °C for the specimens cured at $T = 10$ °C and $T = 45$ °C and then the equivalent age $\tau(t; T, T_{ref})$ of the *in situ* concrete as well as the value of *in situ* concrete strength $f_c(t; T, T_{ref})$ (see Figure 21). We clearly see the logarithmic model trend of the compressive strength with the equivalent time whatever the temperature. The calculation is possible for all regions equipped with a temperature sensor. [47].

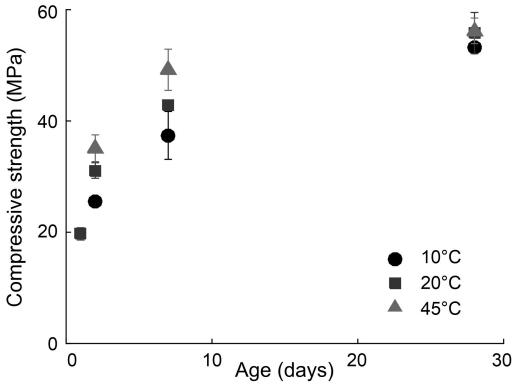

Figure 20: Compressive strength of concrete specimens as a function of the time t for three different curing temperatures $T = 10\ ^\circ\text{C}$, $20\ ^\circ\text{C}$ (T_{ref}) and $45\ ^\circ\text{C}$.

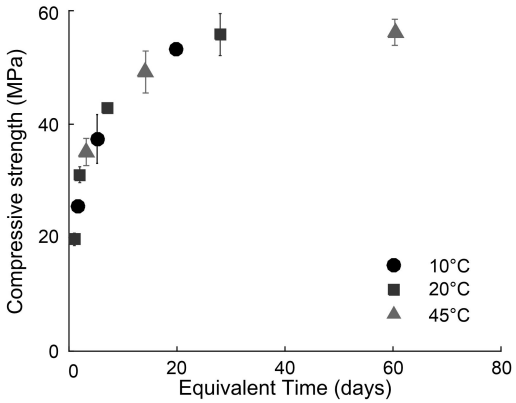

Figure 21: Compressive strength $f_c(t; T, T_{ref})$ of concrete specimens as a function of the equivalent time $\tau(t; T, T_{ref})$ for three different curing temperatures $T = 10\ ^\circ\text{C}$, $20\ ^\circ\text{C}$ (T_{ref}) and $45\ ^\circ\text{C}$.

5.3. *Evolution of average resistivity*

First, we analyze the evolution of the average apparent resistivity measured in the volume below a resistivity sensor. The apparent resistivity measurements in beam 1, under the RS21 and RS22 sensors, has thus been plotted over time in Figure 22. The average of the 117 measurements made with a sensor is calculated to obtain the constituent points of this curve. The error bar symbolizes the standard deviation of all the resistivity measurements yielded by the considered sensor.

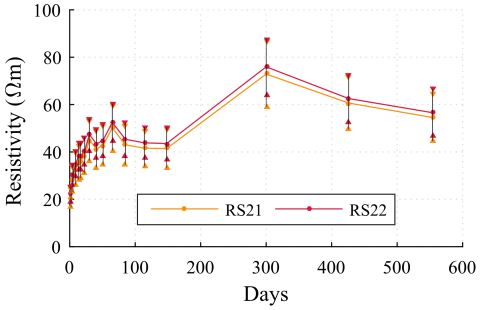

Figure 22: Measured resistivity *in situ* ρ_T.

These data cannot be used directly. The signal is noisy due to thermal effects. It should therefore be corrected. One technique is to calculate the average apparent resistivity at a reference temperature T_{ref} (here 20 °C), according to equation (9):

$$\rho_T = \frac{\rho_{T_{\text{ref}}}}{1 + \alpha\,(T - T_{\text{ref}})} \tag{9}$$

where ρ_T is the apparent resistivity measured at the temperature T and $\rho_{T_{\text{ref}}}$ is the apparent resistivity computed for the temperature T_{ref}. The coefficient α is a correction factor of temperature effects which is set here at 0.022 °C^{-1} as proposed by Whittington and al.[6].

We chose 20 °C for the reference temperature since it is the temperature commonly used in the literature for resistivity correction and also because it is the temperature used for the equivalent time calculation for material hardening. The corrected curves are plotted on Figure 23. After the thermal correction, the resistivity evolutions are similar to those described by the authors who performed resistivity measurement in laboratory on concrete specimens [13, 11]. This result contributes to validate the relevance of the measurements obtained with the *in situ* device and the need for temperature measurement. It can also be noted that the two sensors embedded in the same beam about 20 cm far from each other, give very similar apparent resistivities.

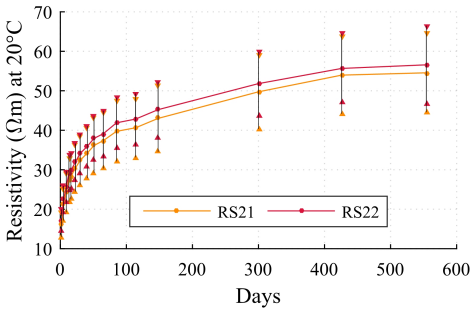

Figure 23: Resistivity $\rho_{T_{\text{ref}}}$ computed at 20 °C.

An interesting property of the resistivity comes from its link to porosity. The porosity evolves with hydration [37] thus modifying the resistivity value. Since, the mechanical strength of concrete is influenced by porosity, the resistivity measurement can be considered as an indicator of material hardening. This appears clearly on Figure 24 on which the mechanical strength is plotted as a function of the average electrical resistivity. The relationship between these two quantities is a linear relationship with a correlation coefficient very close to 1.

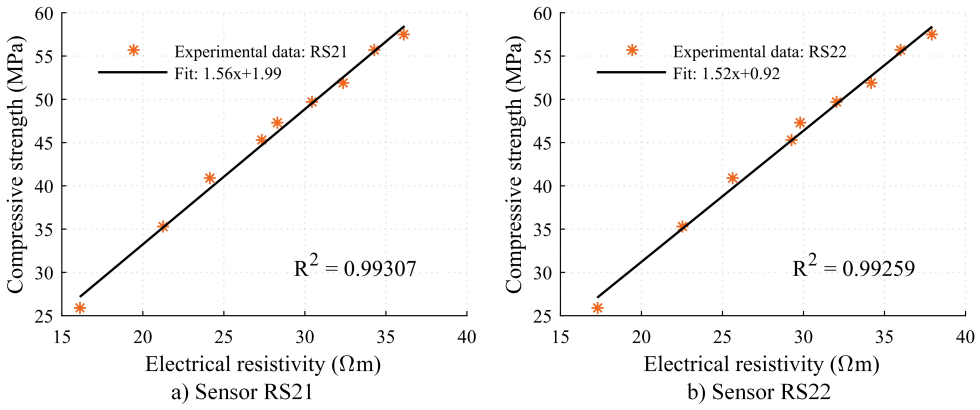

Figure 24: Evolution of compressive strength $f_c(t; T, T_{ref})$ as a fonction of electrical resistivity $\rho_{T_{\text{ref}}}$ for $T_{ref} = 20$ °C.

According to Archie [4], the electrolytic resistivity of the material is given by the following empirical law:

$$\rho = a\rho_w \Phi^{-m} S_r^{-n} \tag{10}$$

with ρ the electrolytic resistivity of concrete (in Ω.m), ρ_w the resistivity of the interstitial

552 solution (temperature dependent), Φ the porosity of the material, S_r the degree of saturation, and
553 where a, m and n are material parameters.

554 In this study it is assumed that the concrete is saturated with water. This assumption seems
555 reasonable considering the environment of the structure and the relative humidity measurements
556 made in the concrete beams. Indeed, the relative humidity variations are low and RH% remains
557 very high over time. So S_r is considered equal to 1 in equation 10.

558 The electrical resistivity of a water-saturated concrete is then a function of the following
559 parameters: pore volume, porous connectivity, cement type (here the same for the two beams),
560 degree of hydration and chemical composition of the pore solution (parameter ρ_w).

561 In a healthy concrete, in the absence of chlorides, the influence of the chemical composition
562 of the pore solution remains small if the solution remains alkaline [36] and thus ρ_w does not
563 vary. The electrical current propagates mainly through the saturated porous network. The most
564 influent parameter on resistivity measurement is therefore the connectivity of the pore network
565 (since the influence of temperature has been previously corrected). The measurement of elec-
566 trical resistivity is therefore a simple way to characterize indirectly the connectivity of a porous
567 saturated medium Φ^{-m}. For a given cement paste, the reduction of porosity due to the hydration
568 of cement results in the same time in a decrease in pore connectivity, and an increase in strength.
569 The morphology of cement paste depends on cement type and concrete composition, thus there
570 is not a general correlation between resistivity and strength (see [48]). Here the same concrete
571 was used for both measurements. This explains the excellent correlation between the mechanical
572 strength measurement and the resistivity measurement observed in Figure 24.

573 On Figure 25, the compressive strength $f_c(t; T, T_{ref})$ is drawn together with the resistivity $\rho_{T_{\text{ref}}}$
574 as a function of equivalent time τ. Both curves exhibit a similar evolution. They have especially
575 similar inflection. As a consequence, when the resistivity has reached its asymptotical value, it
576 can be said that the concrete has almost reached its maximum compressive strength.

577 Simultaneous monitoring of the evolutions of the mechanical properties of concrete and of the
578 resistivity shows that resistivity sensors could be used as part of a strategy to optimize the phasing
579 of the construction process. Obtaining such a result *in situ*, already known and documented in
580 laboratory tests, is particularly interesting because it reinforces the interest of using an embedded
581 resistivity measurement device at early age and not only for chloride assessment. Indeed, both the
582 constructor of the structure, within the framework of the monitoring of manufacturing processes,

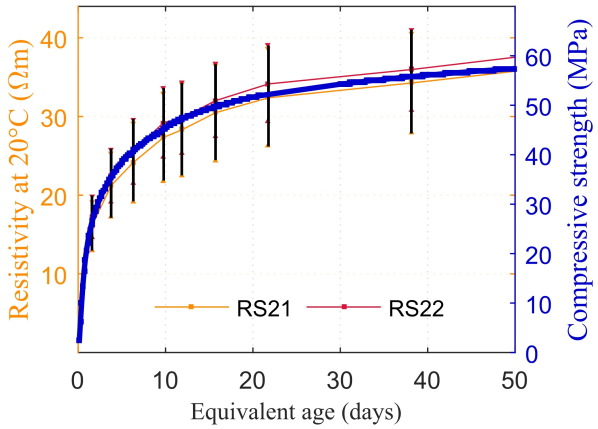

Figure 25: Evolutions of compressive strength $f_c(t; T, T_{ref})$ and of electrical resistivity $\rho_{T_{\text{ref}}}$ as functions of equivalent age τ for $T_{ref} = 20\,^{\circ}\text{C}$.

and the owner of the structure, within the framework of the ageing structure survey, could find an advantage in using this measuring system which reinforces the interest of *in situ* installation of DC measurement devices.

5.4. Displaying the pseudo-sections of apparent resistivities

The pseudo-sections of apparent resistivities displayed following the procedure described in section 4.2 are presented in Figure 26 for days 2, 30 and 426 after concrete casting. The appearance of the pseudo resistivity sections displayed with a given sensor is very similar from one day to another in terms of gradients.

It can also be noted that the dispersion of the resistivity measurements around the mean value is much higher than that observed in the water and also much higher than the repeatability error measured *in situ* in concrete (see section 3.2). The variability of apparent resistivities cannot therefore be explained solely by measurement errors. This variability in resistivity is related to the heterogeneity of the material; the most likely explanation is the variability of porosity. This would explain why the facies of the resistivity maps change only slightly over time once the main chemical reactions have occurred during the very first days of concrete setting and hardening. Conversely, as shown in the previous section, the average resistivity value increases with time which is also consistent with the porosity evolution.

Furthermore, it can be noted that the values of apparent resistivity are very low. Although it is not possible to state that concrete is saturated with water only on the basis of a relative humidity

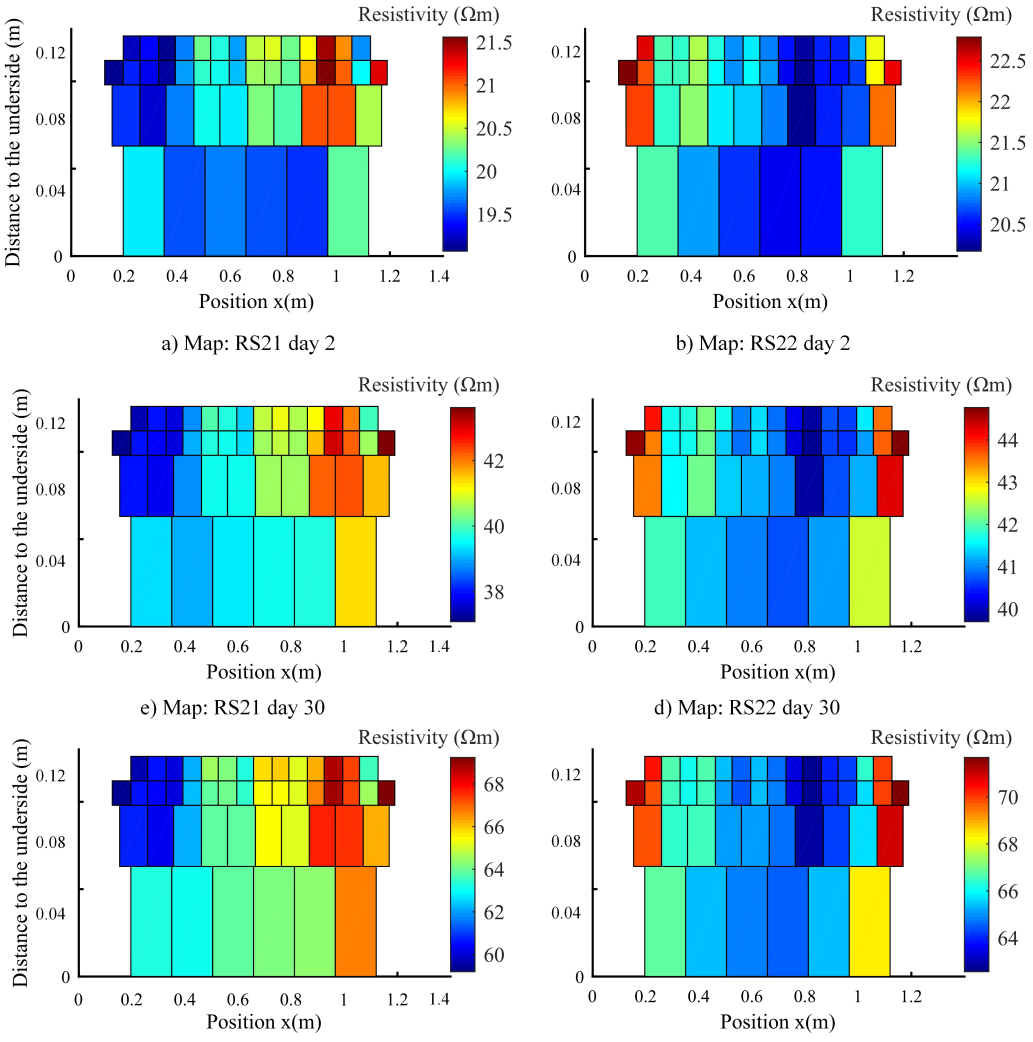

Figure 26: Pseudo sections of resistivity. From left to right: RS21 and RS22 sensors. From top to bottom: days 2, 30 and 426.

measurement in a cavity, the water content of concrete is likely to be very high. This assumption is consistent with the low resistivity values measured on site while the porosity of the concrete measured in laboratory is low (see section 5.2). The values of the resistivities found here are also consistent with the observations of previous work on the topic[13, 49].

An indicator of corrosion probability based solely on the evolution of the average resistivity value does not seem to be the most appropriate choice for application to a port or offshore structure if one refers to the observations made on the wharf (porosity, resistance, relative humidity, temperature and resistivity measurement). Since a pseudo section of apparent resistivity appears to be a characteristic of the material properties in a given area, it is proposed to study the difference between the pseudo sections at two different times. This difference is shown on the Figure 27 on which the resistivity difference obtained for the two sensors RS21 and RS22 on days 114 and 148 is displayed (difference and relative difference).

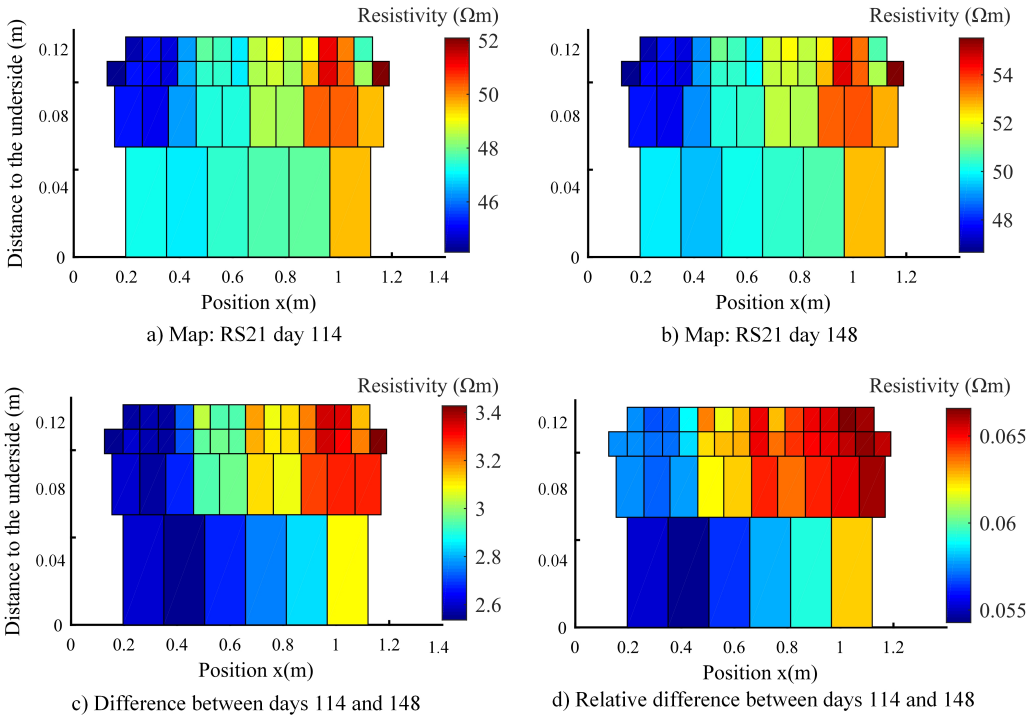

Figure 27: Pseudo section of difference of resistivity. Left: difference of the resistivity of the RS21 sensor between the days 114 and 148. Right: relative difference of the resistivity of the RS21 sensor between the days 114 and 148.

The difference between the apparent resistivities measured on days 114 and 148 is positive

at any point of the pseudo section of apparent resistivity. This is an expected result and this result was found for all ages and sensors. Over time, the water content of concrete is expected to decrease rapidly after the dormant period and then to decrease more and more slowly as the hydration of cement consumes water. A local decrease in resistivity between two time periods (excluding artifacts related to poor temperature compensation) would mean that the concrete has become wetter or that its chemical composition has changed (for example, due to chloride ion penetration). The sign of the difference between two pseudo sections of apparent resistivity appears to be a good indicator of early detection of corrosion. It should be noted, however, that with a pseudo section of apparent resistivity, it would not be possible to accurately define the size of the affected area and its precise distance from the surface. However, this is a good indicator to state almost instantly, - within the framework of a sensor integrated into an SHM chain - and with great certainty that concrete is evolving and that monitoring in the area must be strengthened. Further actions could then be done. In some cases coring concrete specimens could be necessary.

6. Conclusion and outlook

Electrical resistivity measurements are currently used in the field of inspection of civil engineering structure, mainly as part of a one-time measurement campaign using portable Wenner probes. The performance of these devices is limited by the difficulty of obtaining repeatable contact between the electrode and the concrete surface on the one hand and by the presence of reinforcement on the other hand. The intrinsic heterogeneity of concrete also complicates the analysis of measurements, making it difficult to interpret localized measurements.

Embedded sensors in concrete structures during casting solves the problem of poor repeatability measurement induced by resistance contact between concrete and electrode. However, the problem of taking into account the influence of the presence of reinforcements on the measurement remains. This topic is the subject of current work with variable solutions depending on the nature and geometry of the measuring device used [13, 50, 30]. The first objective of this paper was to propose an installation methodology of a multi-electrode sensor embedded in concrete to avoid the influence of reinforcements on measurements. To that aim, the resistivity sensor was attached to a wire mesh that confines the electric current in the concrete cover area. In this study, we chose to use a multi-electrode sensor about one meter long interrogated with a Wenner alpha

protocol to obtain a hundred resistivity measurements in the monitoring area. All the measures available thus allow the intrinsic heterogeneities of the concrete studied to be taken into account. The evolution of the average resistivity value over time was compared with the evolution of the mechanical strength of *in situ* concrete estimated using the maturometry method. This *in situ* result tends to prove the relevance of the proposed method of sensor installation and calibration and also opens the perspective to use resistivity measurement, not only within the framework of ageing survey but also within the framework of concrete hardening monitoring for the optimization of the construction process.

Then, the second goal of this article was to propose a method for analyzing and displaying resistivity measurements in the form of a pseudo section of apparent resistivity. It is based on the numerical evaluation of the sensitivity of potential measurements to resistivity variations in predefined volume blocks according to their influence on the measurements. The methodology has been validated and applied to the analysis of resistivity measurements performed on a new port wharf for 18 months. The heterogeneous and random nature of the resistivity was attributed to the heterogeneity of the porosity of the concrete. It was thus considered that these maps presented information intrinsic to each studied zone and proposed an indicator of corrosion probability based on the study of the difference between two pseudo-sections of apparent resistivity. Since it allows instant visualization of results, the display of apparent resistivity maps can be integrated into an *in situ* measurement system or into a structure supervision system. If an anomaly is detected by comparing the apparent resistivity sections between two days, several actions can be taken, including coring or computation of the true resistivity for a more accurate location of the anomaly. In this case, the apparent resistivity can be used for initialization in the optimization algorithms for the identification of the true resistivity. With the methodology proposed here, it is possible to provide a set of initial parameters close to the final solution, which contributes to improving the efficiency of inversion algorithms.

Resistivity is an indirect indicator of corrosion. When the resistivity value is below a threshold value, the probability of corrosion initiation is considered high. The use of on-site resistivity is in most cases limited to the detection of risk areas. To obtain reliable information on the corrosion of the reinforcement and the position of the chloride front, destructive tests (chloride titration) are traditionally carried out.

It is possible to further exploit the information provided by the resistivity measurement in

order to characterize the degree of corrosion, through the relationships between:

- the resistivity value and the chloride content [51];
- the resistivity value and the value of the diffusion coefficient of chloride ions in concrete [38, 14] ;
- the resistivity value and the current corrosion value [52].

Associated together, the value of the chloride rate in a given area and the diffusion coefficient of chloride in concrete make it possible to obtain predictions over structure life duration by calculation [52].

The measurement of the corrosion current is a direct indicator. It will be interesting during the service life of the structure to compare the resistivity measurements and the predicted advance of the chloride front with measurements of reinforcement electric potential. This study will be the continuation of this work.

Acknowledgment

The authors would like to thank all the partners of iMAREO2 project: Keops Automation (D. Follut, D. Olivier), Université de Nantes (M. Roche), Nantes – Saint Nazaire Port (P. Lijour, M. Labegorre) and Bouygues Construction (the teams of Bouygues Travaux Publics Régions France). The authors would like to thank the Pays de la Loire region for its financial support.

References

[1] Harsh K. Gupta, editor. *Encyclopedia of Solid Earth Geophysics*. Encyclopedia of Earth Sciences Series. Springer Netherlands, 2011.

[2] M.H. Loke. Electrical imaging surveys for environmental and engineering studies A practical guide to 2-D and 3-D surveys. Technical report, 2000.

[3] W.M. Telford, P.L. Geldart, and R.E. Sheriff. *Applied geophysics 2nd edition | Solid earth geophysics*. Cambridge University Press, 1991.

[4] G. E. Archie. The Electrical Resistivity Log as an Aid in Determining Some Reservoir Characteristics. *Transactions of the AIME*, 146(01):54–62, December 1942.

[5] G. E. Archie. Classification of Carbonate Reservoir Rocks and Petrophysical Considerations. *AAPG Bulletin*, 36(2):278–298, 1952.

[6] H. W. Whittington, J. McCarter, and M. C. Forde. The conduction of electricity through concrete. *Magazine of Concrete Research*, 33(114):48–60, March 1981.

[7] Samuel Naar. *Evaluation non destructive du beton par mesures de resistivite electrique et thermographie infrarouge passive*. thesis, Bordeaux 1, January 2006.

[8] J.F. Lataste, C. Sirieix, D. Breysse, and M. Frappa. Electrical resistivity measurement applied to cracking assessment on reinforced concrete structures in civil engineering. *NDT & E International*, 36(6):383–394, September 2003.

[9] Zhiyong Liu, Yunsheng Zhang, and Qian Jiang. Continuous tracking of the relationship between resistivity and pore structure of cement pastes. *Construction and Building Materials*, 53:26–31, February 2014.

[10] M. Saleem, M. Shameem, S. E. Hussain, and M. Maslehuddin. Effect of moisture, chloride and sulphate contamination on the electrical resistivity of Portland cement concrete. *Construction and Building Materials*, 10(3):209–214, April 1996.

[11] Wolfgang Brameshuber, Christoph Dauberschmidt, Petra Schroder, and Michael Raupach. Non-destructive determination of the water content in the concrete cover using the multi-ring-electrode. Technical Report RWTH-CONV-006116, DGZfP, 2003.

[12] Effect of moisture content on concrete resistivity measurement. *Journal of the Chinese Institute of Engineers*, 25:117–122, January 2002.

[13] Rob B Polder. Test methods for on site measurement of resistivity of concrete a rilem tc-154 technical recommendation. *Construction and Building Materials*, 15(2):125–131, March 2001.

[14] Rob B Polder and Willy H. A Peelen. Characterisation of chloride transport and reinforcement corrosion in concrete under cyclic wetting and drying by electrical resistivity. *Cement and Concrete Composites*, 24(5):427–435, October 2002.

[15] W Morris, A Vico, M Vazquez, and S. R de Sanchez. Corrosion of reinforcing steel evaluated by means of concrete resistivity measurements. *Corrosion Science*, 44(1):81–99, January 2002.

[16] Jean-François Lataste. *Évaluation non destructive de l'état d'endommagement des ouvrages en béton armé par mesures de résistivité électrique*. Bordeaux 1, January 2002.

[17] C Andrade, M Castellote, and R d'Andrea. Chloride aging factor of concrete measured by means of resistivity. Porto Portugal, April 2011.

[18] Yann Lecieux, Franck Schoefs, Stéphanie Bonnet, Trystan Lecieux, and Sergio Palma Lopes. Quantification and uncertainty analysis of a structural monitoring device: detection of chloride in concrete using DC electrical resistivity measurement. *Nondestructive Testing and Evaluation*, 30(3):216–232, July 2015.

[19] Yanbo Liu, Francisco Presuel-Moreno, and Mario Paredes. Determination of Chloride Diffusion Coefficients in Concrete by Electrical Resistivity Method. *ACI Materials Journal*, 112(5), October 2015.

[20] Milia Fares, Géraldine Villain, Stéphanie Bonnet, Sergio Palma Lopes, Benoit Thauvin, and Mickael Thiery. Determining chloride content profiles in concrete using an electrical resistivity tomography device. *Cement and Concrete Composites*, 94:315–326, November 2018.

[21] Pejman Azarsa and Rishi Gupta. Electrical Resistivity of Concrete for Durability Evaluation: A Review. *Advances in Materials Science and Engineering*, 2017:1–30, 2017.

[22] Jean-François Lataste, Géraldine Villain, and Jean-Paul Balayssac. Electrical Methods. In *Non-Destructive Testing and Evaluation of Civil Engineering Structures*, pages 139–172. Elsevier, 2018.

[23] R. du Plooy, S. Palma Lopes, G. Villain, and X. Dérobert. Development of a multi-ring resistivity cell and multi-electrode resistivity probe for investigation of cover concrete condition. *NDT & E International*, 54(Supplement C):27–36, March 2013.

[24] W. J. McCarter, T. M. Chrisp, G. Starrs, P. A. M. Basheer, and J. Blewett. Field monitoring of electrical conductivity of cover-zone concrete. *Cement and Concrete Composites*, 27(7):809–817, August 2005.

[25] J.F. Lataste, T. De Larrard, F. Benboudjema, and J. Semenadisse. Study of electrical resistivity: variability assessment on two concretes: protocol study in laboratory and assessment on site. *European Journal of Environmental and Civil Engineering*, 16(3-4):298–310, April 2012.

[26] J-F. Lataste and D. Breysse. A Study on the Variability of Electrical Resistivity of Concrete. In Gunes Oguz and Yillmaz Akkaya, editors, *Nondestructive Testing of Materials and Structures*, pages 255–261. Springer Netherlands, Dordrecht, 2013.

[27] Lucas Bourreau. *Diagnostic de corrosion sur ouvrage : fiabilite et aide a la decision*. Nantes, December 2017.

[28] Ueli M. Angst and Rob Polder. Spatial variability of chloride in concrete within homogeneously exposed areas. *Cement and Concrete Research*, 56:40–51, February 2014.

[29] S G Millard and WENNER. REINFORCED CONCRETE RESISTIVITY MEASUREMENT TECHNIQUES. *Proceedings of the Institution of Civil Engineers*, 91(1):71–88, March 1991.

[30] Gabriel Samson, Fabrice Deby, Jean-Luc Garciaz, and Jean-Louis Perrin. A new methodology for concrete resistivity assessment using the instantaneous polarization response of its metal reinforcement framework. *Construction and Building Materials*, 187:531–544, October 2018.

[31] T. M. Chrisp, G. Starrs, W. J. McCarter, E. Rouchotas, and J. Blewett. Temperature-conductivity relationships for concrete: An activation energy approach. *Journal of Materials Science Letters*, 20(12):1085–1087, 2001.

[32] Marta Castellote, Carmen Andrade, and Mari Cruz Alonso. Standardization, to a Reference of 25 C, of Electrical Resistivity for Mortars and Concretes in Saturated or Isolated Conditions. *Materials Journal*, 99(2):119–128, March 2002.

[33] N. Wiwattanachang and P.H. Giao. Monitoring crack development in fiber concrete beam by using electrical resistivity imaging. *Journal of Applied Geophysics*, 75(2):294–304, October 2011.

[34] P. K. Mehta. CONCRETE. STRUCTURE, PROPERTIES AND MATERIALS. 1986.
[35] RILEM Technical Committee 108. *Interfacial transition zone in concrete: state-of-the-art report*. E & FN Spon, London New York, 1996.
[36] Véronique Baroghel-Bouny. Conception des bétons pour une durée de vie donnée des ouvrages. Technical report, Association Française de Génie Civil, 2004.
[37] Nicolas Burlion, Frédéric Bourgeois, and Jian-Fu Shao. Effects of desiccation on mechanical behaviour of concrete. *Cement and Concrete Composites*, 27(3):367–379, March 2005.
[38] Ozkan Sengul. Use of electrical resistivity as an indicator for durability. *Construction and Building Materials*, 73:434–441, December 2014.
[39] Laboratoire central des ponts et chaussees. *Resistance du beton dans l'ouvrage: la maturometrie*. LCPC, Paris, 2003. OCLC: 54835566.
[40] A. G. A. Saul. Principles underlying the steam curing of concrete at atmospheric pressure. *Magazine of Concrete Research*, 2(6):127–140, March 1951.
[41] European Committee for Standardisation. Eurocode 2: Design of concrete structures - Part 1-1: General rules and rules for buildings, 2004.
[42] P Freiesleben Hansen and E.J. Pedersen. Maleinstrument til Kontrol af betons haerdning. *Nordisk betong*, 1:21–25, 1977.
[43] Jean Paul Balayssac and Vincent Garnier. *Non-destructive Testing and Evaluation of Civil Engineering Structures - 1st Edition*. ISTE Press - Elsevier, 2017.
[44] I.M Sobol. Global sensitivity indices for nonlinear mathematical models and their monte carlo estimates. *Mathematics and Computers in Simulation*, 55(1-3):271–280, 2001.
[45] A. Saltelli, P. Annoni, I. Azzini, F. Campolongo, M. Ratto M., and S. Tarantola. Variance based sensitivity analysis of model output. design and estimator for the total sensitivity index. *Computer Physics Communications*, 181:259–270, 2010.
[46] Bruno Sudret. Global sensitivity analysis using polynomial chaos expansions. *Reliability Engineering & System Safety*, 93(7):964 – 979, 2008. Bayesian Networks in Dependability.
[47] Tahsin Alper Yikici and Hung-Liang (Roger) Chen. Use of maturity method to estimate compressive strength of mass concrete. *Construction and Building Materials*, 95(Supplement C):802–812, October 2015.
[48] Ali Akbar Ramezanianpour, Amirreza Pilvar, Mahdi Mahdikhani, and Faramarz Moodi. Practical evaluation of relationship between concrete resistivity, water penetration, rapid chloride penetration and compressive strength. *Construction and Building Materials*, 25(5):2472–2479, May 2011.
[49] A. Lubeck, A.L.G. Gastaldini, D.S. Barin, and H.C. Siqueira. Compressive strength and electrical properties of concrete with white Portland cement and blast-furnace slag. *Cement and Concrete Composites*, 34(3):392–399, March 2012.
[50] Mustafa Salehi, Pouria Ghods, and O. Burkan Isgor. Numerical investigation of the role of embedded reinforcement mesh on electrical resistivity measurements of concrete using the Wenner probe technique. *Materials and Structures*, 49(1-2):301–316, January 2016.
[51] W Morris, A Vico, and M Vazquez. Chloride induced corrosion of reinforcing steel evaluated by concrete resistivity measurements. *Electrochimica Acta*, 49(25):4447–4453, October 2004.
[52] Michael D. A. Thomas and Phil B. Bamforth. Modelling chloride diffusion in concrete: Effect of fly ash and slag. *Cement and Concrete Research*, 29(4):487–495, April 1999.